Journal of Sound and Vibration (2000) **235**(1), 43–61
doi:10.1006/jsvi.1999.2911, available online at http://www.idealibrary.com on IDEAL®

NUMERICAL ANALYSES ON DYNAMIC CONTROL OF FIVE-DEGREE-OF-FREEDOM MAGLEV VEHICLE MOVING ON FLEXIBLE GUIDEWAYS

XIAO JING ZHENG, JIAN JUN WU AND YOU-HE ZHOU

Department of Mechanics, Lanzhou University, Lanzhou 730000, *People's Republic of China.*
E-mail: zhouyh@lzu.edu.cn

(*Received* 14 *September* 1999, *and in final form* 20 *December* 1999)

This paper presents numerical analyses on dynamic behavior of a maglev vehicle with a control system moving on flexible guideways. The vehicle is simplified as a body with the primary and the secondary suspension parts and has five-degree-of-freedom (d.o.f.). So, its five kinds of motions, i.e., heave, sway, pitch, roll, and yaw motions are considered. The numerical results show that the dynamical characteristics of a coupling maglev vehicle/guideway system are different from those of the uncoupling system in which the deformation of the guideways is neglected. For the coupling system, one kind of disturbances in the five motions may excite several other kinds of moving responses. Both the disturbances and the control parameters have an influence on the stability of the dynamical system. In order to make the system stable, regions for the disturbance of heave motion or/and sway motion and the control parameters are numerically searched in detail.

1. INTRODUCTION

As a new type of transportation on ground, a high-speed vehicle which is magnetically levitated (maglev) has been proposed to meet future requirements of, for example, inter-city transportation since the 1970s [1–5]. At present, some practical tests of maglev vehicles in Japan and Germany show that a forward velocity of the vehicle may reach up to or over 500 km/h which is the highest one in all transportation tools on ground. For this kind of vehicles, some mechanical characteristics including dynamical responses of vehicle, vibration of guideways, and bearing capacity to a disturbance of motions, etc. have to be considered in a concept design of maglev vehicles in order to guarantee the safety and ride quality [5–8].

Chu and Moon [4] proposed a two-degree-of-freedom (d.o.f.) vehicle model in which the transverse motion to the guideway (sway) and the rotation motion about the vertical axis (yaw) were considered. Divergence and flutter were demonstrated by their experiments and their theoretical model. Chiu *et al.* [6] and Katz *et al.* [7] studied the dynamic characteristic of flexible guideways under magnetic suspension forces. Recently, Cai *et al.* [8, 9] and Cai and Chen [10] numerically conducted some analyses on dynamic responses of a maglev vehicle, the guideway and their interaction. For the vehicle, Cai and Chen [10] suggested a three- and five-d.o.f. models in which various experimentally measured magnetic force data were incorporated. Instabilities of the vehicle were observed from their analytical and numerical solutions. For the guideway, the Bernoulli–Euler beam theory is used to describe the dynamic responses of the period guideways [8]. The vehicle was considered as a moving

0022-460X/00/310043 + 19 $35.00/0

force travelling at various speeds on a simply supported single or two span beam(s). Dynamic interactions between the guideway and the vehicle were also studied by Cai *et al.* [8, 9], in which the vehicle was, respectively, considered to be a concentrated load [8] and a multicar, multiload [9] with two-d.o.f., and the magnetic suspension forces exerted on the vehicle are not considered. Some very useful conclusions are obtained in their researches.

It is obvious that there exist at least three sub-systems, e.g., the vehicle motion, vibration of guideways, and a control system for generating controllable maglev forces in a coupling maglev vehicle/guideway system. It has been found that their interactions have strongly influenced the dynamic stability of the system. Although the stability of dynamic control for a magnetic suspension body on an undeformable ferromagnetic guideway was studied by Moon [5], Meisenholder *et al.* [11], and Zhou and Zheng [12], no research has been found to give a theoretical analysis for a coupling maglev vehicle/guideway system with controllable maglev forces.

In this paper, a theoretical model for a coupling five-d.o.f. maglev vehicle/guideway system with a controllable feedback magnetic force is presented to investigate the dynamic behavior of motions of vehicle, vibration of guideways, and control stability. The maglev force applied on the vehicle is analytically calculated. With the aid of the Runge–Kutta–Merson method [13], a numerical code is proposed to simulate responses of the non-linear dynamical system. By comparing the responses of the coupling system with these of the uncoupling system, it is found that the responses of the coupling system are different from those of the uncoupling one for the same situations, i.e. the same geometric and material parameters, the same control law and parameters, etc.. The effects of each motion disturbance on responses of the coupling dynamical system with controllable forces are displayed in a case study. The numerical results indicate that the stability of the system is influenced by both the control parameters and the disturbances. That is, on the one hand, for a given disturbance, the dynamical system may be stable by means of choosing a set of control parameters in a certain region; On the other hand, for a set of given control parameters, the dynamical system may be stable when a disturbance is not beyond a critical value. The dependence between the control parameters and the heave or/and sway motion disturbances is numerically searched when the coupling dynamical system is hopefully controlled to be stable.

2. GOVERNING EQUATIONS

2.1. ANALYSIS ON FORCE SYSTEM

The system of a five-d.o.f. maglev vehicle studied here is shown in Figure 1. For the guideways, the span length, the bending rigidity and the damping coefficient are, respectively, denoted by l, EJ and C_g. The maglev vehicle is simplified as four same "magnetic wheels" and a mass lump consisting of a bogie and a car body. The magnetic wheels and the mass lump are joined by springs and dampers. Here, the electromagnetic attraction forces in the heave and the sway directions are generated from the magnetic circuit between the magnetic wheels and the ferrous rails, which are controlled by the electric circuits of a control system. The magnetic wheels and the mass lump are, respectively, called the primary suspension bodies and the secondary suspension body, which are identified by the superscripts "1" and "2" respectively. The geometrical parameters of the mass lump are denoted by $a^{(2)} \times b^{(2)} \times h^{(2)}$, and the masses of the mass lump and each of the four magnetic wheels are represented by $m^{(2)}$ and $m^{(1)}$ respectively. It is assumed that the springs and the dampers are linear, to which the spring coefficients and

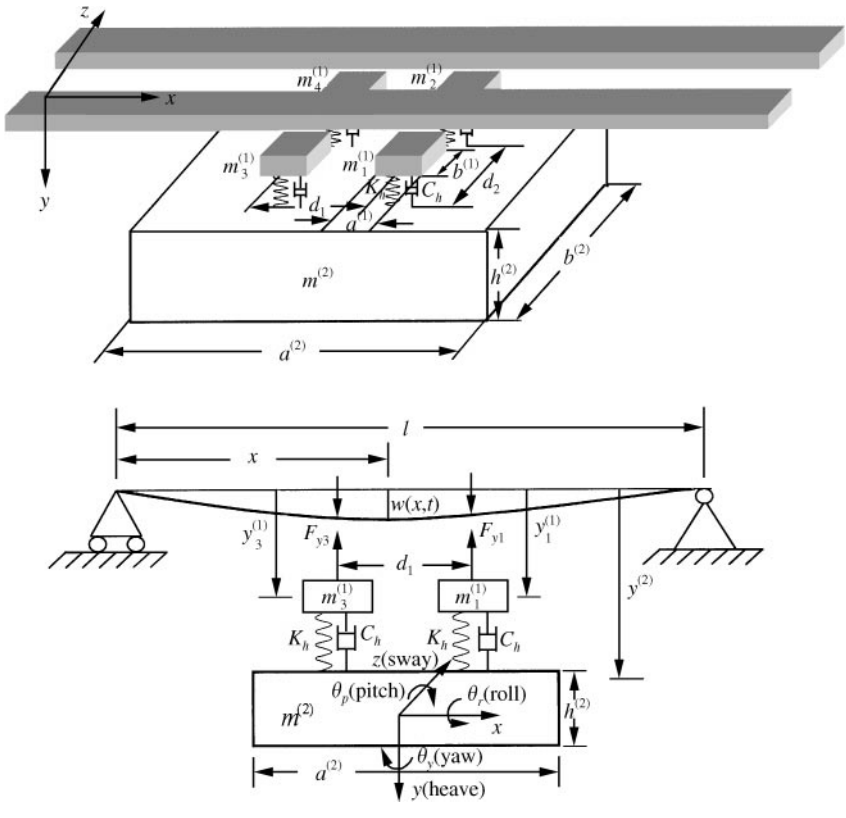

Figure 1. Schematic diagram of a Maglev vehicle guideway system.

damping coefficients are denoted by K_β and C_β ($\beta = h, s, p, y, r$ which are the abbreviations of heave, sway, pitch, yaw, and roll respectively). From the control system of magnetic suspension, we know that a magnetic circuit which can be controlled is composed of the magnetic wheels, the ferromagnetic guideways and the air region between the wheels and the guideways. The electric resistance and the equivalent magnetic reluctances are represented by R and $R_\alpha^*(t)$ ($\alpha = 1, 2, 3, 4$) respectively. The rated area of a magnetic pole, or magnetic wheel, is denoted by $A_0 = a_\alpha^{(1)} \times b_\alpha^{(1)}$. Let $w(t, x)$ be the deflection of guideways at position x and instant of time t, and $w_\alpha^*(t)$ be the deflection of the guideways at the position of the αth magnetic wheel. And $y_\alpha^{(1)}, z_\alpha^{(1)}(\alpha = 1, 2, 3, 4)$ and $y^{(2)}, z^{(2)}$ are, respectively, the co-ordinates of the primary and the secondary suspension bodies in the $oxyz$ co-ordinate system shown in Figure 1. According to the linear spring and damping relations, and the formula of magnetic forces [5], we have the following:

Restoring spring forces:

$$K_h(y^{(2)} - y_\alpha^{(1)}), \qquad K_s(z^{(2)} - z_\alpha^{(1)}) \quad (\alpha = 1, 2, 3, 4). \tag{1}$$

Viscous damping forces:

$$C_h(\dot{y}^{(2)} - \dot{y}_\alpha^{(1)}), \qquad C_s(\dot{z}^{(2)} - \dot{z}_\alpha^{(1)}) \quad (\alpha = 1, 2, 3, 4). \tag{2}$$

Magnetic forces:

$$F_{y\alpha} = \frac{\phi_\alpha^2(t)}{\mu_0 A_\alpha}, \qquad F_{z\alpha} = -\frac{\phi_\alpha^2(t)}{\pi}\frac{a^{(1)} z_\alpha^{(1)}}{\mu_0 A_\alpha^2} \quad (\alpha = 1, 2, 3, 4), \tag{3}$$

where $F_{y\alpha}$ and $F_{z\alpha}$ indicate the components of magnetic forces in the heave and the sway directions respectively. Here, the dot "$\cdot$" represents "$\mathrm{d}/\mathrm{d}t$", μ_0 is the magnetic permeability of vacuum, $A_\alpha = a_\alpha^{(1)} \times (b_\alpha^{(1)} - z_\alpha^{(1)})$ ($\alpha = 1, 2, 3, 4$) are the effective areas of magnetic pole, and ϕ_α is the magnetic flux at magnetic pole α, which is related to the magnetic reluctances R_α^*:

$$\phi_\alpha(t) = \frac{NI_\alpha(t)}{R_\alpha^*} \quad (\alpha = 1, 2, 3, 4) \tag{4}$$

in which N is the number of turns of coil, I_α represents the control current in the electric circuit, and

$$R_\alpha^* = R_0^* + r^* s_\alpha(t) \quad (\alpha = 1, 2, 3, 4). \tag{5}$$

Here, $r^* = 2/\mu_0 A_0$, $s_\alpha(t) = \delta_\alpha(t) - \delta_0$ is the disturbance along the y-axis, R_0^* stands for the effective magnetic reluctance between the magnetic wheel and the rail at the static equilibrium state of the magnetic suspension with control goal of air gap δ_0, and δ_α denotes the air gap of the form

$$\delta_\alpha(t) = y_\alpha^{(1)}(t) - w_\alpha^*(t) \quad (\alpha = 1, 2, 3, 4). \tag{6}$$

2.2. DYNAMICAL EQUATIONS

Applying the momentum law and the angular momentum law to the primary and the secondary suspension bodies as shown in Figure 1, we can write

Equations of motions of Maglev vehicle

$$m^{(1)}\ddot{y}_\alpha^{(1)} - C_h(\dot{y}^{(2)} - \dot{y}_\alpha^{(1)}) - K_h(y^{(2)} - y_\alpha^{(1)}) = m^{(1)}g - F_{y\alpha} \quad (\alpha = 1, 2, 3, 4), \tag{7}$$

$$m^{(1)}\ddot{z}_\alpha^{(1)} - C_s(\dot{z}^{(2)} - \dot{z}_\alpha^{(1)}) - K_s(z^{(2)} - z_\alpha^{(1)}) = F_{z\alpha} \quad (\alpha = 1, 2, 3, 4), \tag{8}$$

$$m^{(2)}\ddot{y}^{(2)} + C_h \sum_{\alpha=1}^{4} (\dot{y}^{(2)} - \dot{y}_\alpha^{(1)}) + K_h \sum_{\alpha=1}^{4} (y^{(2)} - y_\alpha^{(1)}) = m^{(2)}g, \tag{9}$$

$$m^{(2)}\ddot{z}^{(2)} + C_s \sum_{\alpha=1}^{4} (\dot{z}^{(2)} - \dot{z}_\alpha^{(1)}) + K_s \sum_{\alpha=1}^{4} (z^{(2)} - z_\alpha^{(1)}) = 0, \tag{10}$$

$$J_p\ddot{\theta}_p + C_p\ddot{\theta}_p + K_p\theta_p = (J_r - J_y)\dot{\theta}_r\dot{\theta}_y + L_p, \tag{11}$$

$$J_y\ddot{\theta}_y + C_y\dot{\theta}_y + K_y\theta_y = (J_p - J_r)\dot{\theta}_p\dot{\theta}_r + L_y, \tag{12}$$

$$J_r\ddot{\theta}_r + C_r\dot{\theta}_r + K_r\theta_r = (J_y - J_p)\dot{\theta}_y\dot{\theta}_p + L_r, \tag{13}$$

in which the double dot "··" represents "$\mathrm{d}^2/\mathrm{d}t^2$", and θ_p, θ_y and θ_r are the Euler's angles which describe the rotations of pitch, yaw and roll respectively. The first terms on the right-hand side of equations (11)–(13) indicate the components of the vector product of angular velocity vector and angular momentum vector of the secondary suspension body in the rotation axes of pitch, yaw and roll motions, respectively, which is generated from the difference between time derivatives of the angular momentum vector of the body about the (fixed) space axes and the (moving) body axes, and J_p, J_y and J_r are the moments of inertia of the vehicle about the rotation axes of pitch, yaw, and roll motions, respectively, i.e.,

$$J_p = \tfrac{1}{12} m^{(2)}[(a^{(2)})^2 + (h^{(2)})^2], \qquad J_y = \tfrac{1}{12} m^{(2)}[(a^{(2)})^2 + (b^{(2)})^2],$$

$$J_r = \tfrac{1}{12} m^{(2)}[(h^{(2)})^2 + (b^{(2)})^2], \tag{14}$$

and L_p, L_y and L_r are the force moments about the rotation axes of pitch, yaw and roll motions respectively. They are

$$L_p = \frac{d_1}{2}\left[C_h(\dot{y}_4^{(1)} + \dot{y}_3^{(1)} - \dot{y}_2^{(1)} - \dot{y}_1^{(1)}) - K_h(y_4^{(1)} + y_3^{(1)} - y_2^{(1)} - y_1^{(1)})\right]\cos\theta_p, \tag{15}$$

$$L_y = \frac{d_1}{2}\left[C_s(\dot{y}_4^{(1)} + \dot{y}_3^{(1)} - \dot{y}_2^{(1)} - \dot{y}_1^{(1)}) - K_s(y_4^{(1)} + y_3^{(1)} - y_2^{(1)} - y_1^{(1)})\right]\cos\theta_y, \tag{16}$$

$$L_r = \frac{d_2}{2}\left[C_h(\dot{y}_4^{(1)} - \dot{y}_3^{(1)} + \dot{y}_2^{(1)} - \dot{y}_1^{(1)}) - K_h(y_4^{(1)} - y_3^{(1)} + y_2^{(1)} - y_1^{(1)})\right]\cos\theta_r. \tag{17}$$

By the Bernoulli–Euler beam theory for the bending deformation of the guideways, we have

Deflection equation:

$$EJ\frac{\partial^2 w}{\partial x^4} + C_g\frac{\partial w}{\partial t} + \rho\frac{\partial^2 w}{\partial t^2} = \eta_1(t,x)\sum_{\alpha=1}^{2} F_{y\alpha}(t)/a_\alpha^{(1)} + \eta_2(t,x)\sum_{\alpha=3}^{4} F_{y\alpha}(t)/a_\alpha^{(1)} \tag{18}$$

in which

$$\eta_2(t,x) = \begin{cases} 1 & vt - \dfrac{a^{(1)}}{2} \leqslant x \leqslant vt + \dfrac{a^{(1)}}{2}, \\ 0 & \text{else}, \end{cases} \tag{19}$$

$$\eta_2(t,x) = \begin{cases} 1 & vt - d_1 - \dfrac{a^{(1)}}{2} \leqslant x \leqslant vt - d_1 + \dfrac{a^{(1)}}{2}, \\ 0 & \text{else}. \end{cases} \tag{20}$$

Here, $a^{(1)} = a_\alpha^{(1)}$. According to the circuit equivalence of Faraday's law, we get

Control equations:

$$N\frac{\mathrm{d}\phi_\alpha(t)}{\mathrm{d}t} = -RI_\alpha(t) + V_\alpha(t) \quad (\alpha = 1, 2, 3, 4), \tag{21}$$

where V_α are the control voltages which generate the control currents I_α to stabilize the maglev vehicle.

Corresponding to the control goal of levitation gap δ_0 which is pre-specified hopefully, we denote the bias current by I_0 provided by a constant voltage $V_{\alpha,0}$ in the electric circuit α. Then, we may further denote

$$\phi_{\alpha,0} = \frac{NI_0}{R_0^*} \quad (\alpha = 1, 2, 3, 4), \tag{22}$$

$$V_{\alpha,0} = RI_0 \quad (\alpha = 1, 2, 3, 4), \tag{23}$$

$$I_\alpha(t) = I_0 + \mathrm{i}_\alpha(t) \quad (\alpha = 1, 2, 3, 4), \tag{24}$$

$$V_\alpha(t) = V_{\alpha,0} + V_{\alpha,c}(t) \quad (\alpha = 1, 2, 3, 4). \tag{25}$$

Following Meisenholder and Wang [11] and Moon [5], we choose the following control law:

$$V_{\alpha,c}(t) = G_1 s_\alpha(t) + G_2 \dot{s}_\alpha(t) \quad (\alpha = 1, 2, 3, 4), \tag{26}$$

where G_1 and G_2 are the gains of control parameters. According to equations (3)–(6) and (22), and applying the equilibrium equation to vehicle in the vertical direction, one may get a dependence of I_0 of the form

$$\sum_{\alpha=1}^{4} \frac{(NI_0/R_0^*)^2}{\mu_0 A_\alpha} = (4m^{(1)} + m^{(2)})g. \tag{27}$$

Substituting equations (4) and (26) into equation (21), and considering equations (5), (6), (23)–(25), and (27), when $|s_\alpha(t)| \ll 1$, we can obtain

$$\frac{\mathrm{d}i_\alpha}{\mathrm{d}t} = \frac{1}{N^2}\left[G_1(y_\alpha^{(1)} - \omega_\alpha^* - \delta_0) + G_2(\dot{y}_\alpha^{(1)} - \dot{w}_\alpha^*) - Ri_\alpha\right]\left[R_0^* + r^*(y_\alpha^{(1)} - w_\alpha^* - \delta_0)\right]$$

$$+ \frac{r^*(\dot{y}_\alpha^{(1)} - \dot{w}_\alpha^*)(I_0 + i_\alpha)}{R_0^* + r^*(y_\alpha^{(1)} - \omega_\alpha^* - \delta_0)} \quad (\alpha = 1, 2, 3, 4). \tag{28}$$

Thus, equations (7)–(13), (18) and (28) constitute the governing equations of a maglev vehicle/guideway system with controllable maglev forces. In these basic equations, the maglev forces given by equation (3) can be written as

$$F_{y\alpha} = \left(m^{(1)} + \frac{1}{4}m^{(2)}\right) g \frac{A_0}{a_\alpha^{(1)}(b_\alpha^{(1)} - z_\alpha^{(1)})} \frac{(1 + i_\alpha/I_0)^2}{(1 + r^*/R_0^*(y_\alpha^{(1)} - \omega_\alpha^* - \delta_0))^2} \quad (\alpha = 1, 2, 3, 4), \tag{29a}$$

$$F_{z\alpha} = -\frac{1}{\pi}\left(m^{(1)} + \frac{1}{4}m^{(2)}\right) g \frac{A_0 z_\alpha^{(1)}}{a_\alpha^{(1)}(b_\alpha^{(1)} - z_\alpha^{(1)})^2} \frac{(1 + i_\alpha/I_0)^2}{(1 + r^*/R_0^*(y_\alpha^{(1)} - \omega_\alpha^* - \delta_0))^2} \quad (\alpha = 1, 2, 3, 4). \tag{29b}$$

It is obvious from equation (29) that maglev forces $F_{y\alpha}$ and $F_{z\alpha}$ ($\alpha = 1, 2, 3, 4$) are non-linearly dependent on the deflection of guideways and the vehicle motions. Besides that, they are non-linearly dependent on the control current so that they are controllable by adjusting the gains of control parameters G_1 and G_2. Therefore, the basic equations proposed in this paper to describe the dynamic behavior of the maglev vehicle/guideway system are non-linear and simultaneous partial differential equations about unknown control currents and unknown displacements.

3. SOLUTION METHOD

For the purpose of simplicity in the numerical analysis of dynamic characteristics to the control system, here, we introduced the following dimensionless quantities:

$$\bar{y}_\alpha^{(1)} = \frac{y_\alpha^{(1)}}{l}, \quad \bar{y}^{(2)} = \frac{y^{(2)}}{l}, \quad \bar{z}_\alpha^{(1)} = \frac{z_\alpha^{(1)}}{l}, \quad \bar{z}^{(2)} = \frac{z^{(2)}}{l}, \quad \bar{d}_1 = \frac{d_1}{l}, \quad \bar{d}_2 = \frac{d_2}{l}, \quad \bar{w} = \frac{w}{l},$$

$$\bar{w}^* = \frac{w^*}{l}, \quad \bar{a}^{(1)} = \frac{a^{(1)}}{l}, \quad \bar{b}^{(1)} = \frac{b^{(1)}}{l}, \quad \bar{a}^{(2)} = \frac{a^{(2)}}{l}, \quad \bar{b}^{(2)} = \frac{b^{(2)}}{l}, \quad \bar{h}^{(2)} = \frac{h^{(2)}}{l}, \quad \bar{\delta}_0 = \frac{\delta_0}{l},$$

$$\bar{g} = \frac{gl}{v^2}, \quad \bar{i}_\alpha = \frac{i_\alpha}{I_0}, \quad \bar{\rho} = \frac{\rho l}{m^{(1)}}, \quad \bar{E} = \frac{El^3}{m^{(1)}v^3}, \quad \bar{C}_g = \frac{C_g l^2}{m^{(1)}v}, \quad \bar{J} = \frac{J}{l^4}, \quad \bar{m}^{(2)} = \frac{m^{(2)}}{m^{(1)}},$$

$$\bar{t} = \frac{tv}{l}, \quad \bar{G}_1 = \frac{G_1 l^2 I_0}{m^{(1)}v^3}, \quad \bar{G}_2 = \frac{G_2 l I_0}{m^{(1)}v^2}, \quad \bar{R} = \frac{RlI_0^2}{m^{(1)}v^3}, \quad \bar{R}_0^* = \frac{R_0^* m^{(1)}v^2}{I_0^2},$$

$$\bar{r}^* = \frac{r^* m^{(1)}v^2}{lI_0^2}, \quad \bar{C}_{\beta_1} = \frac{C_{\beta_1} l}{m^{(1)}v}, \quad \bar{K}_{\beta_1} = \frac{K_{\beta_1} l^2}{m^{(1)}v^2}, \quad \bar{C}_{\beta_2} = \frac{C_{\beta_2}}{m^{(1)}lv}, \quad \bar{K}_{\beta_2} = \frac{K_{\beta_2}}{m^{(1)}v^2}$$

$$(\beta_1 = h, s, \beta_2 = p, y, r), \tag{30}$$

After that, the dynamic and control equations of equations (7)–(13), (18) and (28) may be reduced into ones with dimensionless form. For the dimensionless partial differential equation corresponding to the bending equation (18) of guideways, we use the method of modal analysis in which

$$\bar{w}(\bar{x}, \bar{t}) = \sum_{n=1}^{N} Y_n(\bar{t})\, \Phi_n(\bar{x}). \tag{31}$$

Here $\Phi_n(\bar{x})$ is the orthonormal modal function of order n for the free vibration of the guideways. For example, when the guideways are simply supported at the ends of a single span, we have

$$\Phi_n(\bar{x}) = \sin n\pi\bar{x}. \tag{32}$$

And $Y_n(\bar{t})$ is the nth modal co-ordinate to be determined. Substituting equations (31) into the dimensionless bending equation of the guideways, and applying the Galerkin method, one can get a set of ordinary differential equations with unknowns $Y_n(n = 1, 2, 3, \ldots, N)$. At the following quantitative analysis, we take $N = 5$ because the numerical test shows that when $N = 5$, the numerical solution for the deflection function has enough accuracy if we focus on those vibrations of the guideways with low frequency.

For simplicity in expression, we will omit the bar over each dimensionless quantity if there is no obscure understanding. For example, we use w for $\bar{w}$. Once we denote

$$x_{2k-1} = y_\alpha^{(1)}, \quad x_{2k} = \dot{y}_\alpha^{(1)}, \quad x_{2k+9} = z_\alpha^{(1)}, \quad x_{2k+10} = \dot{z}_\alpha^{(1)}, \quad x_{26+k} = \dot{i}_\alpha, \quad (k = \alpha = 1, 2, 3, 4),$$

$$x_9 = y^{(2)}, \quad x_{10} = \dot{y}^{(2)}, \quad x_{19} = z^{(2)}, \quad x_{20} = \dot{z}^{(2)}, \quad x_{21} = \theta_p, \tag{33}$$

$$x_{22} = \dot{\theta}_p, \quad x_{23} = \theta_y, \quad x_{24} = \dot{\theta}_y, \quad x_{25} = \theta_r, \quad x_{26} = \dot{\theta}_r,$$

$$x_{30+2j-1} = Y_j, \quad x_{30+2j} = \dot{Y}_j \quad (j = 1, 2, \ldots, 5),$$

the dimensionless equations of the dynamical control system can be rewritten by the matrix form in state space as

$$\frac{\mathrm{d}\mathbf{X}(t)}{\mathrm{d}t} = \mathbf{A}(t)\mathbf{X}(t) + \mathbf{F}(t) + \mathbf{C}. \tag{34}$$

Here, $\mathbf{A}(t)$ is a matrix of order 40×40 (see Appendix A), and

$$\mathbf{X}(t) = [x_1, x_2, \ldots, x_{40}]^{\mathrm{T}}, \tag{35a}$$

$$\mathbf{F}(t) = [\mathbf{F}_1^{\mathrm{T}}, \mathbf{F}_2^{\mathrm{T}}, \mathbf{F}_3^{\mathrm{T}}, \mathbf{0}^{\mathrm{T}}, \mathbf{0}^{\mathrm{T}}]^{\mathrm{T}}, \tag{35b}$$

$$\mathbf{C} = [\mathbf{C}_1^{\mathrm{T}}, \mathbf{0}^{\mathrm{T}}, \mathbf{C}_3^{\mathrm{T}}, \mathbf{C}_4^{\mathrm{T}}, \mathbf{C}_5^{\mathrm{T}}]^{\mathrm{T}}, \tag{35c}$$

in which

$$\mathbf{F}_1 = [0, -F_{y1}, 0, -F_{y2}, 0, -F_{y3}, 0, -F_{y4}, 0, 0]^{\mathrm{T}},$$

$$\mathbf{F}_2 = [0, -F_{z1}, 0, -F_{z2}, 0, -F_{z3}, 0, -F_{z4}, 0, 0]^{\mathrm{T}}, \quad \mathbf{F}_3 = [0, L_p/J_p, 0, L_y/J_y, 0, L_r/J_r]^{\mathrm{T}},$$

$$\mathbf{C}_1 = [0, g, 0, g, 0, g, 0, g, 0, g]^{\mathrm{T}}, \qquad \mathbf{C}_3 = [0, \Gamma_p, 0, \Gamma_y, 0, \Gamma_r]^{\mathrm{T}},$$

$$\mathbf{C}_4 = [-\Gamma_3 G_1 A_0, -\Gamma_3 G_1 A_0, -\Gamma_3 G_1 A_0, -\Gamma_3 G_1 A_0]^{\mathrm{T}},$$

$$\mathbf{C}_5 = [0, \Gamma_4(4r^* A_0/R_0^* + 2)(\eta_1 + \eta_2), \ldots, 0, \Gamma_4(4r^* A_0/R_0^* + 2)(\eta_1 + \eta_2)]^{\mathrm{T}},$$

and

$$\Gamma_1 = (1 + \tfrac{1}{4} m^{(2)}) g b^{(1)}, \qquad \Gamma_2 = G_2 + N^2 r^*/R_0^{*2}, \qquad \Gamma_3 = R_0^*/N^2,$$

$$\Gamma_4 = (1 + \tfrac{1}{4} m^{(2)}) g/(\rho a^{(1)}), \qquad \Gamma_5 = (1 + \tfrac{1}{4} m^{(2)}) g b^{(1)}/\pi,$$

$$\Gamma_p = \frac{J_r - J_y}{J_p} \dot{\theta}_r \dot{\theta}_y, \qquad \Gamma_y = \frac{J_p - J_r}{J_y} \dot{\theta}_p \dot{\theta}_r \qquad \Gamma_r = \frac{J_y - J_p}{J_r} \dot{\theta}_y \dot{\theta}_p,$$

where $b^{(1)} = b_\alpha^{(1)}$. From equation (34), it is found that the dynamic control system is governed by a set of ordinary differential equations with variable coefficients.

4. NUMERICAL RESULTS AND DISCUSSIONS

In order to quantitatively simulate the characteristics of the coupling control system described in the previous sections, some numerical method has to be employed. Here, the Runge–Kutta–Merson method [13] of numerical integrals is applied to equation (34) such that the roundoff error in the numerical method may be avoided. Based on this numerical code, a numerical example is given to understand the characteristics of the dynamical control system. Table 1 lists the parameters of the system of the numerical example.

First of all, the dynamic responses of the coupling vehicle/guideway system and the uncoupling system are, respectively, simulated when a small heave disturbance $y_0^{(2)} = 8{\cdot}0 \times 10^{-4}$ on the initial displacement of the car body is pre-given. The numerical results demonstrate that when the guideway deformation is ignored, or vehicle/guideway system is uncoupling, only the heave motion is excited, and the vehicle quickly reaches its stable steady state if the control parameters G_1 and G_2 are taken in the stable region of this dynamical system. Once the deflection of the guideways is considered in the dynamical system, however, the four kinds of motions, i.e., heave, pitch, roll, and yaw, of the car body are excited simultaneously (see Figure 2). The excited responses in the coupling maglev vehicle guideway system vary with moving velocity v for a given disturbance and the given control parameters. With the increase of the velocity v, the maximum displacement increases before $v \leqslant v_c/2$ and decreases after $v \geqslant v_c/2$. Here v_c is the one order characteristic velocity of the vehicle, i.e., $v_c = (\pi/l)\sqrt{EJ/\rho}$ (ρ is the mass density of the guideway). Figure 3 exhibits the different stability characteristics of the maglev systems. When $G_1 = 1{\cdot}0 \times 10^5$, $G_2 = 3{\cdot}0 \times 10^6$, $v = 150$ m/s, the heave flutter, shown in Figure 3.1, is found for both the coupling and the uncoupling systems when an initial heave disturbance $y_{\alpha 0}^{(1)} = 4{\cdot}0 \times 10^{-4}$ is given. By adjusting G_2 into $G_2 = 2{\cdot}0 \times 10^7$, the uncoupling system becomes stable, but the coupling maglev vehicle/guideway system is still unstable.

Next, the effects of one kind of disturbance in the five motions on the responses of the coupling maglev vehicle/guideway system are simulated for $v = 150$ m/s, which are plotted in Figure 4. The numerical results indicate that one kind of disturbance may not only have an influence on its own motion, but also excite several other motions of the vehicle. For example, a disturbance of sway motion may excite all five motions. However, a rotation disturbance, such as pitch, roll, and yaw motions, has influence only on the rotation

TABLE 1

Geometric and material parameters of the maglev system

K_h	8·0E + 5 kg/s	l	25 m	$m^{(1)}$	1000 kg
C_h	5·0E + 5 kg/s^2	ρ	1500 kg/m	$m^{(2)}$	20000 kg
K_s	2·0E + 4 kg/s	C_g	0·05 kg/m s	$a^{(1)}$	1·0 m
C_s	3·0E + 3 kg/s^2	EJ	3·78E + 9 N/m^2	$a^{(2)}$	8·5 m
K_p	8·0E + 5 kg m^2/s^2	R	1 Ω	$b^{(1)}$	0·028 m
C_p	2·0E + 4 m^2/s	R_0^*	200 A/wb	$b^{(2)}$	3·3 m
K_y	1·0E + 5 kg m^2/s^2	I_0	28 A	$h^{(2)}$	3·0 m
C_y	2·0E + 4 m^2/s	δ_0	0·01 m	d_1	6·5 m
K_r	1·0E + 5 kg m^2/s^2	A_0	0·028 m^2	d_2	3·5 m
C_r	2·0E + 4 m^2/s	N	320		

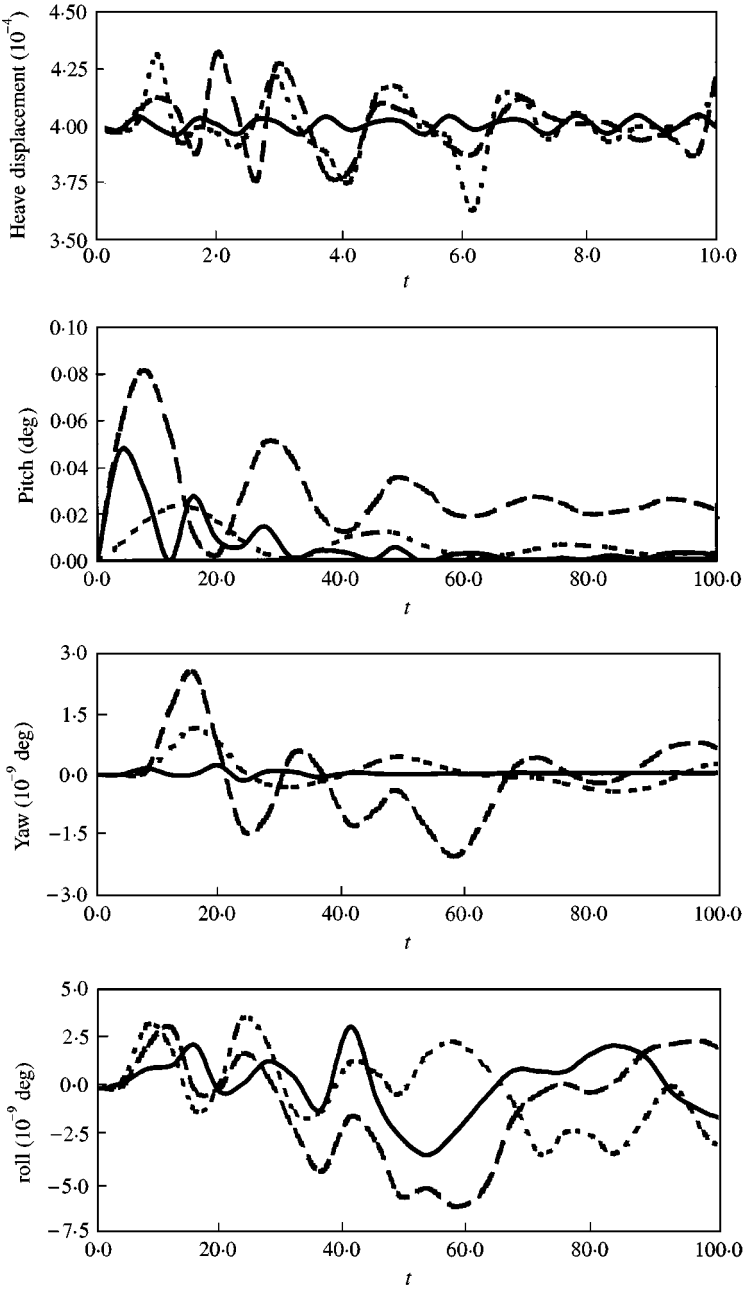

Figure 2. Four kinds of moving responses for vehicle guideway coupling system: ——— $v = 50{\cdot}0$ m/s; — — — $v = 100{\cdot}0$ m/s; - - - - $v = 150{\cdot}0$ m/s.

motions. These results tell us that the effects of a disturbance of linear displacements are greater than that of a disturbance of angular displacements.

Finally, the effects of magnitude of a disturbance, moving velocity, and control parameters on dynamical stability of the controlled maglev vehicle/guideway system are

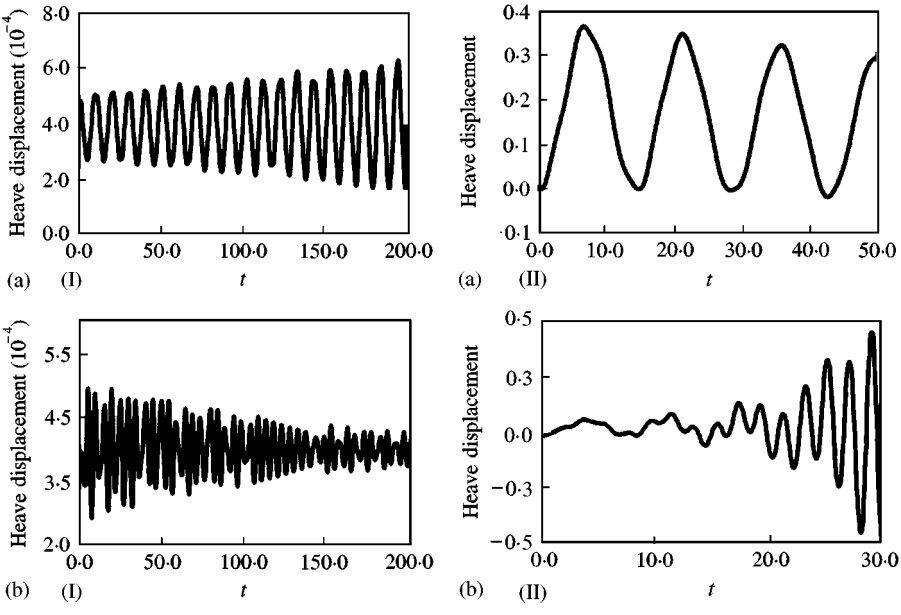

Figure 3. Response curves of uncoupling and coupling systems for control parameters ($v = 150$ m/s). (a) $G_1 = 1{\cdot}0 \times 10^5$, $G_2 = 3{\cdot}0 \times 10^6$; (I) uncoupling system; (II) coupling system, (b) $G_1 = 1{\cdot}0 \times 10^5$, $G_2 = 2{\cdot}0 \times 10^7$; (I) uncoupling system; (II) coupling system.

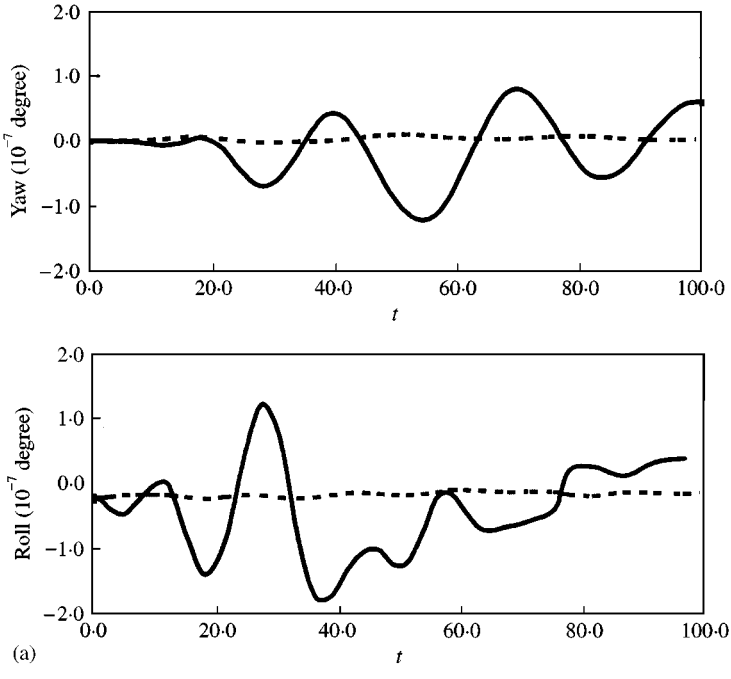

Figure 4. Moving responses of coupling system on different disturbances ($v = 150$ m/s). (a) Heave disturbance, (b) sway disturbance, (c) pitch disturbance, (d) yaw disturbance, (e) roll disturbance: - - - - no disturbance, ——— with disturbance.

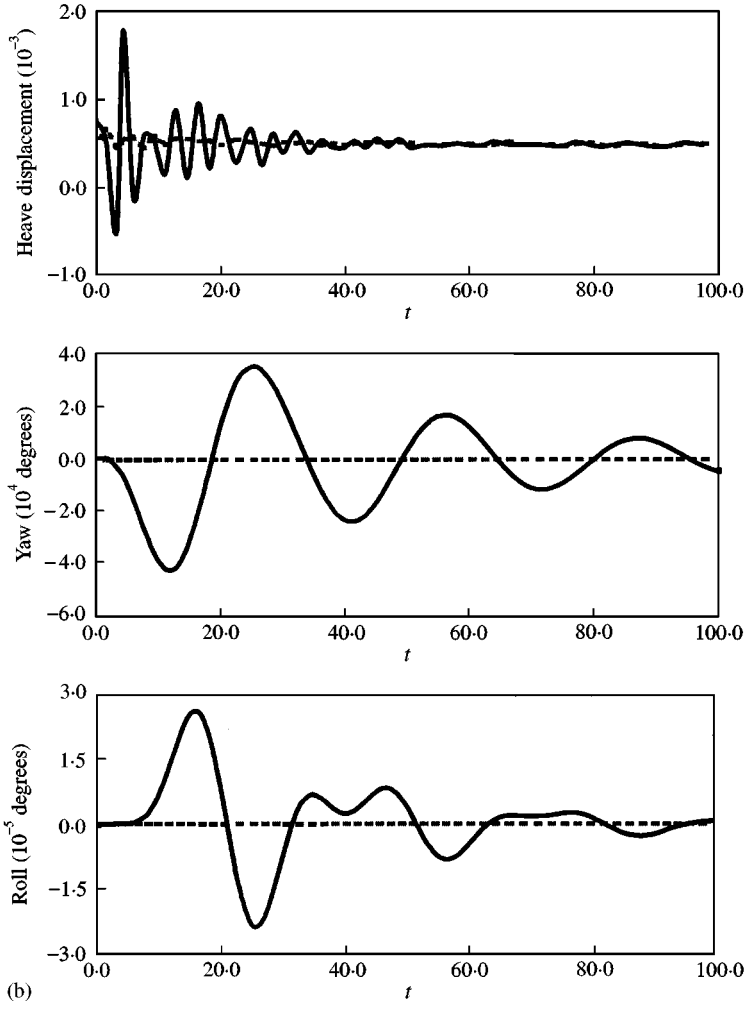

Figure 4. Continued.

discussed. When $v = 150$ m/s and control parameters $G_1 = 8{\cdot}0 \times 10^5$ and $G_2 = 1{\cdot}0 \times 10^7$, the numerical simulations demonstrate that the vehicle will collide with the guideway for a heave disturbance $y_{\alpha 0}^{(1)} = 4{\cdot}8 \times 10^{-4}$ (see Figure 5(a)) and diverge for $y_{\alpha 0}^{(1)} = 5{\cdot}6 \times 10^{-4}$ (see Figure 5(b)). For this situation, the dynamical system can become stable (see Figure 5(c)) as long as we adjust G_2 of the system into $G_2 = 1{\cdot}3 \times 10^7$. Figure 6 plots the effects of moving velocity on the dynamic stability of the controlled system. When the control parameters are taken as $G_1 = 6{\cdot}0 \times 10^5$ and $G_2 = 1{\cdot}0 \times 10^7$, the control system (or the response of heave motion shown in Figure 6) is stable for $v = 50$ m/s, but is unstable for $v = 150$ m/s. Since the magnitude of the disturbance exerted on the vehicle, the velocity and the control parameters G_1 and G_2 play important roles in the dynamic stability of the system, it is necessary to clearly know the dependence of G_1 or G_2 on the disturbances for a given velocity of the system. This kind of dependence is searched in detail for the heave and sway disturbances and shown in Figures 7 and 8, respectively, when $v = 150$ m/s. Figures 7(a) and 8(a),

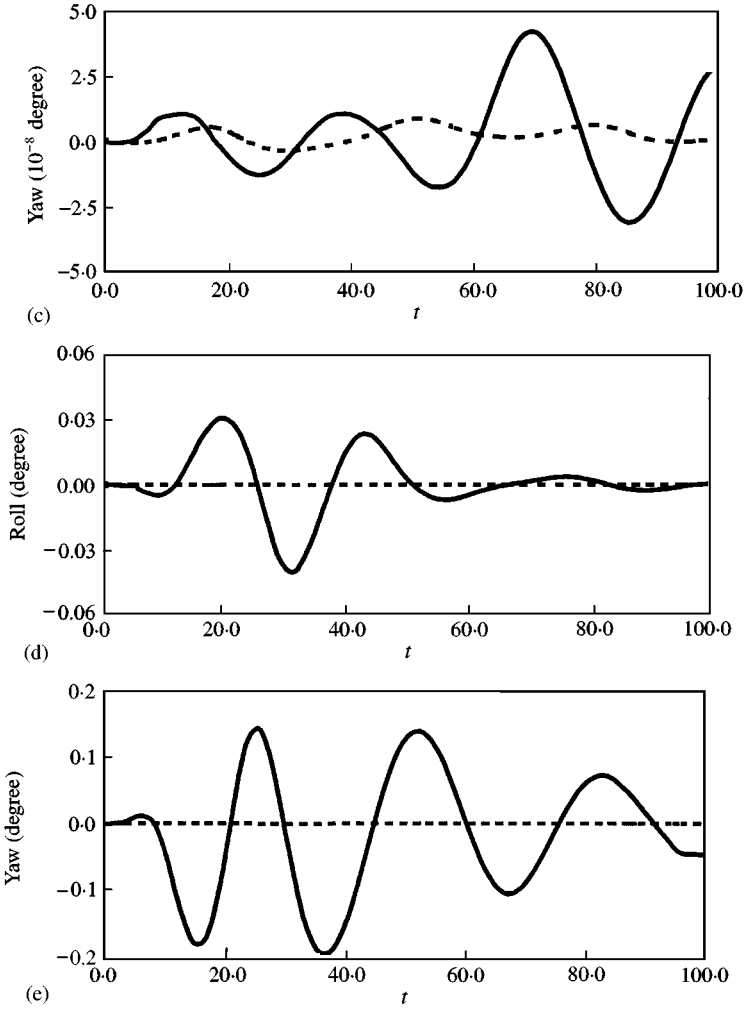

Figure 4. Continued.

respectively, show the curves of the minimum value of G_2 with the magnitudes of the heave and sway disturbances for a given G_1. The numerical simulations demonstrate that when $G_2 \leqslant 9{\cdot}21 \times 10^7$ and G_2 is in the regions under the curves shown in Figures 7(a) and 8(a), the dynamical control system may be controlled, or the system is stable. With the increasing of magnitude of the disturbances, the minimum value G_{2min} has to increase to keep the system stable. However, there exists a critical value of the disturbance for a given system. When the magnitude of the disturbance increases over the critical value, it is difficult to make the system stable no matter how one adjusts G_1 and G_2. For this case, the system is uncontrollable. In addition, for a given G_2, the curves of the maximum value of G_1 with the magnitudes of the heave and sway disturbances are, respectively, shown in Figures 7(b) and 8(b). When $20 < G_1 \leqslant G_{1max}$ and the disturbances are lower than the critical one, the system can be controlled. Combining Figure 7 with Figure 8, we can determine a set of parameters G_1 and G_2 for stable control when the magnitude of the disturbance is under its critical value.

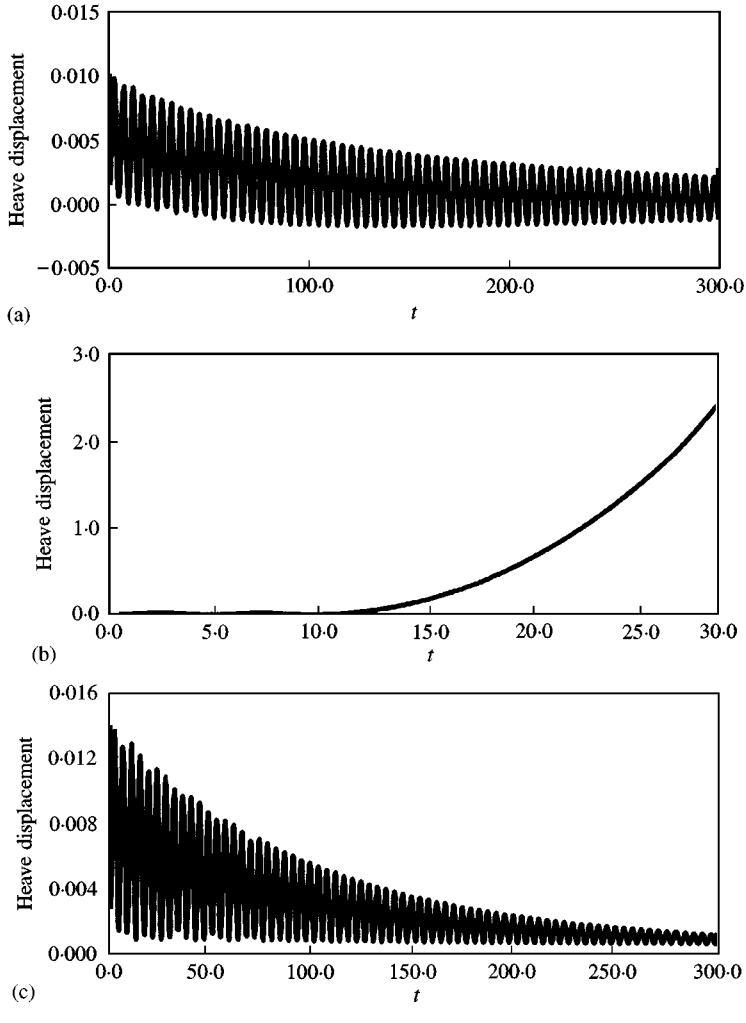

Figure 5. The effects of the suspension gap disturbance on the stability of the coupling system: (a) $y_{z0}^{(1)} = 4{\cdot}8 \times 10^{-4}$, $G_1 = 8{\cdot}0 \times 10^6$, $G_2 = 1{\cdot}0 \times 10^7$; (b) $y_{z0}^{(1)} = 5{\cdot}6 \times 10^{-4}$, $G_1 = 8{\cdot}0 \times 10^6$, $G_2 = 1{\cdot}0 \times 10^7$; (c) $y_{z0}^{(1)} = 4{\cdot}8 \times 10^{-4}$, $G_1 = 8{\cdot}0 \times 10^6$, $G_2 = 1{\cdot}3 \times 10^7$.

5. CONCLUSIONS

This study develops a dynamic interaction model of a maglev vehicle/guideway system under controllable magnetic suspension forces. The vehicle is considered to be with five-degree-of-freedom, which consists of four primary and one secondary suspension bodies jointed by linear springs and dampers. The Bernoulli–Euler beam equation is used to model the characteristic of a flexible guideway. Divergence, flutter and colliding with the guideway are observed by the model and numerical solutions presented in this paper. The numerical results find that the coupling vehicle/guideway system is more sensitive for the motion disturbances than the uncoupling one. System parameters such as the velocity of the vehicle, gain coefficients and applied motion disturbances play very important roles

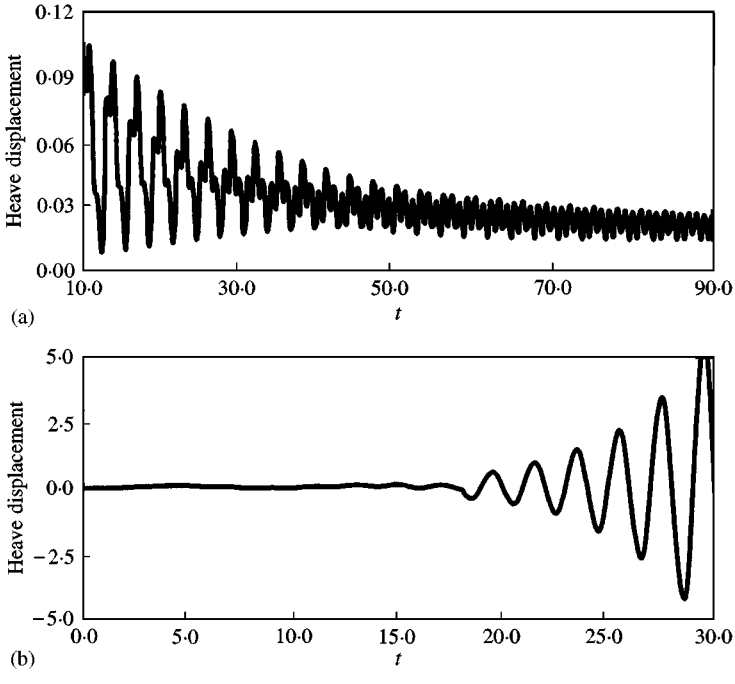

Figure 6. The effects of velocity on the stability of the coupling system: (a) $v = 50{\cdot}0$ m/s; (b) $v = 150{\cdot}0$ m/s.

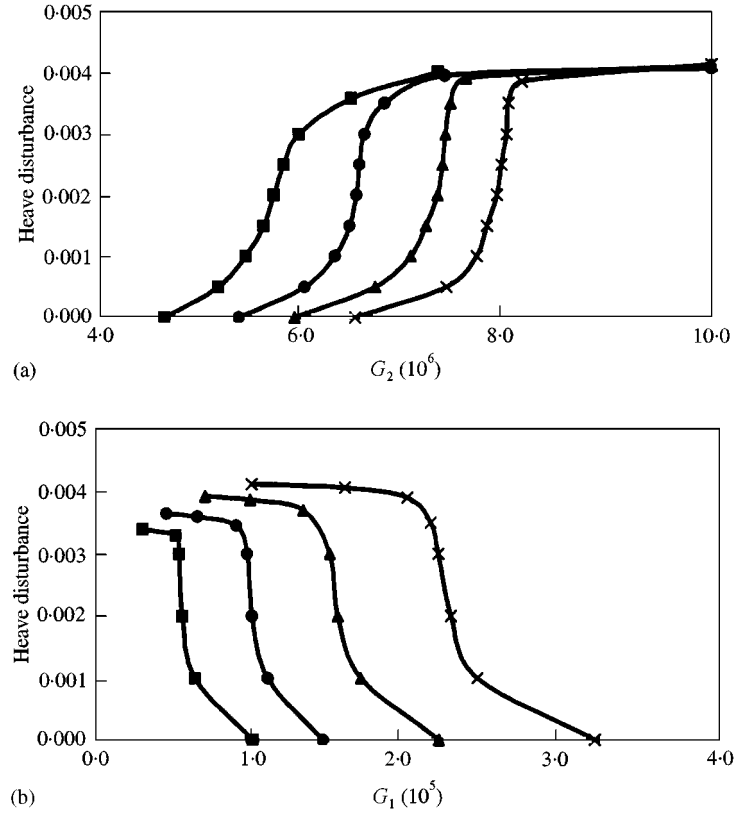

Figure 7. Stability range for heave disturbances: (a) G1 = 1·0E + 5; G1 = 1·5E + 5; G1 = 2·0E + 5; G1 = 2·5E + 5. (b) G2 = 4·5E + 6; G2 = 5·5E + 6; G2 = 6·5E + 6; G2 = 7·5E + 6.

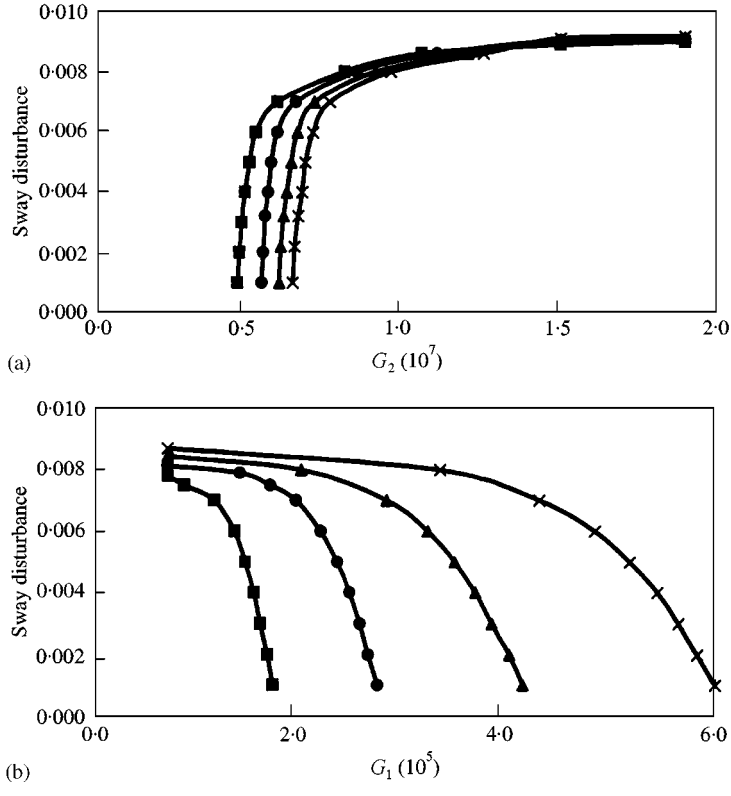

Figure 8. Stability range for sway disturbances: (a) G1 = 1·0E + 5; G1 = 1·5E + 5; G1 = 2·0E + 5; G1 = 2·5E + 5. (b) G2 = 5.5E + 6; G2 = 6·5E + 6; G2 = 7·5E + 6; G2 = 8·5E + 6.

in the dynamic instability of maglev vehicles. The system can be controlled by adjusting the non-linear magnetic suspension force exerted on the system to change conditions of the stability when the system parameters are in stable regions found in this paper.

ACKNOWLEDGMENTS

The authors would like to express their sincere appreciation for the support related to this subject in part by a grant from the National Natural Science Foundation of China for Outstanding Young Researchers (19725207), the Science Foundation of the Ministry of Education of China for Ph.D. Programme, the Foundation of Pre-Research Project of the Defence Committee of Science and Technology of China, and the Opening Foundation of the Chinese State Key Laboratory of Strength and Vibration of Mechanical Structures.

REFERENCES

1. H. T. COFFEY, J. C. SOLINSKY, J. D. COLTON and J. R. WOODBURY 1974 *IEEE Transaction of Magnetism* **MAG 10**, 451–457. Dynamic performance of the SRI maglev vehicle.
2. F. C. MOON 1984 *Magneto-solid Mechanics*. New York: John Wiley & Sons.

3. T. OHTSUKA and Y. KYOTANI 1979 *IEEE Transaction of Magnetism*, **Mag 15**, 1428–1433. Development of high speed surface transport system.
4. D. CHU and F. C. MOON 1983 *Journal of Applied Physics* **54**, 1619–1625. Dynamic instabilities in magnetically levitated models.
5. F. C. MOON 1974 *IEEE Transaction of Magnetism* **Mag 10**, 439–442. Laboratory studies of maglev levitation in the thin track limit.
6. W. S. CHIU, R. G. SMITH and D. N. WORMLEY 1971 *Journal of Dynamic System, Measurement and Control, Transaction of the ASME* **93**, 25–34. Influence of vehicle and distributed guideway parameters on high speed vehicle-guideway dynamic interaction.
7. R. M. KATZ, V. D. NENE, R. J. RAVERA and C. A. SKALSKI 1974 *Journal of Dynamic Systems, Measurement and Control, Transaction of the ASME* **106**, 204–212. Performance of magnetic suspensions for high speed vehicles operating over flexible guideways.
8. Y. CAI, S. S. CHEN, D. M. ROTE and H. T. COFFEY 1994 *Journal of Sound and Vibration* **175**, 625–646. Vehicle/guideway interaction for high speed vehicles on a flexible guideway.
9. Y. CAI, S. S. CHEN, D. M. ROTE and H. T. COFFEY 1996 *Journal of Dynamic Systems, Measurement, and Control, Transaction of ASME* **118**, 526–530. Vehicle/guideway dynamic interaction in maglev systems.
10. Y. CAI and S. S. CHEN 1995 *Shock and Vibration* **2**, 339–349. Numerical analysis for dynamic instability of electrodynamic maglev systems.
11. S. G. MEISENHOLDER and T. C. WANG 1972, *U. S. Federal Rail Administration Report No. FRA-RT-73-1*. Dynamic analysis of an electromagnetic suspension system for a suspended vehicle system.
12. Y. H. ZHOU and X. J. ZHENG 1997 *Journal of Vibration Engineering* **10**, 474–479. Dynamic stability of electromagnetic levitation with feedback control (in Chinese).
13. M. KUBIČEK, and M. MAREK 1983 *Computational Methods in Bifurcation Theory and Dissipative Structure*. New York: Springer-Verlag Inc.

APPENDIX A: EXPRESSION OF MATRIX A

$$\mathbf{A}(t) = \begin{bmatrix} \mathbf{A}_1 & & & & \\ & \mathbf{A}_2 & & & \\ & & \mathbf{A}_3 & & \\ \mathbf{A}_4 & & & \mathbf{A}_5 & \\ \mathbf{A}_6 & & & & \mathbf{A}_7 \end{bmatrix}$$

in which

$$\mathbf{A}_1 = \begin{bmatrix} 0 & 1 & & & & & & & 0 & 0 \\ -K_h & -C_h & & & & & & & K_h & C_h \\ & & 0 & 1 & & & & & 0 & 0 \\ & & -K_h & -C_h & & & & & K_h & C_h \\ & & & & 0 & 1 & & & 0 & 0 \\ & & & & -K_h & -C_h & & & K_h & C_h \\ & & & & & & 0 & 1 & 0 & 0 \\ & & & & & & -K_h & -C_h & K_h & C_h \\ & & & & & & & & 0 & 1 \\ \frac{K_h}{m^{(2)}} & \frac{C_h}{m^{(2)}} & & \cdots & & & \frac{K_h}{m^{(2)}} & \frac{C_h}{m^{(2)}} & -\frac{4K_h}{m^{(2)}} & -\frac{4C_h}{m^{(2)}} \end{bmatrix}$$

$$\mathbf{A}_2 = \begin{bmatrix} 0 & 1 & & & & & & & 0 & 0 \\ -K_s & -C_s & & & & & & & K_s & C_s \\ & & 0 & 1 & & & & & 0 & 0 \\ & & -K_s & -C_s & & & & & K_s & C_s \\ & & & & 0 & 1 & & & 0 & 0 \\ & & & & -K_s & -C_s & & & K_s & C_s \\ & & & & & & 0 & 1 & 0 & 0 \\ & & & & & & -K_s & -C_s & K_s & C_s \\ & & & & & & & & 0 & 1 \\ K_s & C_s & & \cdots & & & K_s & C_s & -4K_s & -4C_s \end{bmatrix},$$

$$\mathbf{A}_3 = \begin{bmatrix} 0 & 1 & & & & & \\ -\frac{K_p}{I_p} & -\frac{C_p}{I_p} & & & & & \\ & & 0 & 1 & & & \\ & & -\frac{K_v}{I_y} & -\frac{C_v}{I_y} & & & \\ & & & & 0 & 1 & \\ & & & & -\frac{K_r}{I_r} & -\frac{C_r}{I_r} & \end{bmatrix},$$

$$\mathbf{A}_4 = \begin{bmatrix} \Gamma_3 G_1 & \Gamma_3 \Gamma_2 & & & & & & \\ & & \Gamma_3 G_1 & \Gamma_3 \Gamma_2 & & & & \\ & & & & \Gamma_3 G_1 & \Gamma_3 \Gamma_2 & & \\ & & & & & & \Gamma_3 G_1 & \Gamma_3 \Gamma_2 \end{bmatrix},$$

$$\mathbf{A}_5 = \begin{bmatrix} -\Gamma_3 R & & & & \Delta_1 & 0 & \Delta_2 & 0 & \cdots & \Delta_5 & 0 \\ & -\Gamma_3 R & & & \Delta_1 & 0 & \Delta_2 & 0 & \cdots & \Delta_5 & 0 \\ & & -\Gamma_3 R & & \Delta_1 & 0 & \Delta_2 & 0 & \cdots & \Delta_5 & 0 \\ & & & -\Gamma_3 R & \Delta_1 & 0 & \Delta_2 & 0 & \cdots & \Delta_5 & 0 \end{bmatrix},$$

$$\mathbf{A}_6 = \begin{bmatrix} 0 & 0 & 0 & 0 & 0 & 0 & 0 & 0 \\ -\Gamma_5 \Gamma_4 \eta_1 & 0 & -\Gamma_5 \Gamma_4 \eta_1 & 0 & -\Gamma_5 \Gamma_4 \eta_2 & 0 & -\Gamma_5 \Gamma_4 \eta_2 & 0 \\ \vdots & \vdots & \vdots & \vdots & \vdots & \vdots & \vdots & \vdots \\ 0 & 0 & 0 & 0 & 0 & 0 & 0 & 0 \\ -\Gamma_5 \Gamma_4 \eta_1 & 0 & -\Gamma_5 \Gamma_4 \eta_1 & 0 & -\Gamma_5 \Gamma_4 \eta_2 & 0 & -\Gamma_5 \Gamma_4 \eta_2 & 0 \end{bmatrix},$$

$$\mathbf{A}_7 = \begin{bmatrix} 0 & 0 & 0 & 0 & 0 & 1 & 0 & 0 & \cdots & 0 & 0 \\ 2\Gamma_4\eta_1 & 2\Gamma_4\eta_1 & 2\Gamma_4\eta_2 & 2\Gamma_4\eta_2 & v_1 - \omega_1^2 & -2\xi_1\omega_1 & v_2 & 0 & \cdots & v_5 & 0 \\ 0 & 0 & 0 & 0 & 0 & 0 & 0 & 1 & \cdots & 0 & 0 \\ 2\Gamma_4\eta_1 & 2\Gamma_4\eta_1 & 2\Gamma_4\eta_2 & 2\Gamma_4\eta_2 & v_1 & 0 & v_2 - \omega_2^2 & -2\xi_2\omega_2 & \cdots & v_5 & 0 \\ 0 & 0 & 0 & 0 & 0 & 0 & 0 & 0 & \cdots & 0 & 1 \\ 2\Gamma_4\eta_1 & 2\Gamma_4\eta_1 & 2\Gamma_4\eta_2 & 2\Gamma_4\eta_2 & v_1 & 0 & v_2 & 0 & \cdots & v_5 - \omega_5^2 & -2\xi_5\omega_5 \end{bmatrix},$$

$$\Delta_i = (\Gamma_3\Gamma_2 + \Gamma_3 G_1)\sin i\pi t + \Gamma_3\Gamma_2\pi i\cos i\pi t \quad (i = 1, 2, \ldots, 5),$$

$$v_i = \frac{4R_1}{R_0}\Gamma_4(\eta_1 + \eta_2)\sin i\pi t, \qquad \omega_i = i^2\pi^2\sqrt{EJ/\rho}, \qquad \xi_i = C_g/2\rho\omega_i \quad (i = 1, 2, \ldots, 5).$$